Nanoscience and
Nanotechnology Letters
Vol. 7, 588–593, 2015

The Effects of ZnS Thickness on the Photocatalytic Performance of ZnO/ZnS Heterostructures

Shuo Yang[1, 2], Yunfei Sun[3], Bayanheshig[1], Lili Yang[3], and Jinghai Yang[3, *]

[1] *Changchun Institute of Optics, Fine Mechanics and Physics, Chinese Academy of Sciences, Changchun 130033, China*
[2] *University of Chinese Academy of Sciences, Beijing 100049, China*
[3] *Key Laboratory of Functional Materials Physics and Chemistry of the Ministry of Education, Jilin Normal University, Siping 136000, Jilin, China*

Well aligned ZnO/ZnS heterostructures with different thichness of ZnS layer have been synthesized on ITO substrates by a simple SILAR method. The morphology properties of as grown heterostructures were investigated by SEM and TEM images. From the SEM and TEM results, the thickness of ZnS layer increased with the increased SILAR period. When SILAR period was 10 times, the chickens of ZnS layer was about 24 nm. ZnO/ZnS(10) structure shows the highest photocatalytic activity. Although ZnO/ZnS heterostructures do not show very high photocatalytic activity, ZnO/ZnS heterostructures will attract increased attention due to its multifunction and low cost.

Keywords: ZnO/ZnS Heterostructures, Photocatalysis, Electron Recombination.

1. INTRODUCTION

The environmental problems have become one of the main challenges that human faced. Semiconductor photocatalyst is an efficient approach for environmental decontamination by the chemical utilization of solar energy,[1–3] which is capable of converting the toxic and nonbiodegradable organic compounds into carbon dioxide and inorganic constituents. Zinc oxide, with a wide band gap of 3.37 eV and a large exciton binding energy (60 meV),[4–10] is considered as one of the most promising semiconductor which can be potentially applied in photocatalysis due to its high surface-to-volume ratio, nontoxicity, high photon utilizing efficiency, and diverse morphologies.[11] However, the fast recombination of photogenerated electron–hole pairs seriously affects the photocatalytic efficiency. So, it is necessary to improve the photocatalytic performance of ZnO nanostructure by modification to inhibit recombination of photo generated electron–hole pairs. Great efforts have been made to overcome this problem. ZnO has been successfully incorporated with narrow band gap semiconductors (such as CdS, CdTe, CdSe, CuO, and Fe_2O_3) and some wide band gap semiconductors (such as SnO_2, ZnS, and TiO_2).[12–19]

ZnS is considered as an important II–VI group semiconductor photocatalyst due to the rapid generation of electron–hole pairs by photoexcitation and the highly negative reduction potentials of excited electrons,[4, 20] which is widely applicable for the photodecomposition of various organic substrates.[21] Recently, 1D ZnO/ZnS nanostructures have been reported, exhibiting superior or new functional properties compared with their individual constituent materials.[22] For example, ZnS/ZnO heterostructures have been successfully fabricated by Wu et al., which exhibits improved photocatalytic efficiency due to the reduced volume recombination of the charge carries and the multiple reflection effect.[23] However, there is no report about the effects of ZnS thickness on the performance of ZnO/ZnS heterostructures.

In this work, 1D ZnO nanorods were synthesized by a two-step CBD approach. ZnS shell layer was synthesized by successive ionic layer adsorption and reaction (SILAR) method. ZnO/ZnS was used as photocatalyst, the effects of different ZnS thickness on the performance of heterostructures will be discussed in detail.

2. EXPERIMENTAL METHODS

2.1. Chemicals

In our experiment, all chemicals (analytical grade reagents, 99.0%) were directly used without further purification. Ethanol, acetone, zinc acetate dehydrate ($Zn(C_2H_3O_2)_2 \cdot 2H_2O$), zinc nitrate hexahydrate ($Zn(NO_3)_2 \cdot 6H_2O$) and methenamine ($C_6H_{12}N_4$) were purchased from Guoyao

*Author to whom correspondence should be addressed.

1941-4900/2015/7/588/006 doi:10.1166/nnl.2015.1977

Group Chemical Reagent Shenyang Co. Sodium sulfide 9-hydrate ($Na_2S \cdot 9H_2O$) was obtained from Liaoning Quanrui Reagent Co. All chemicals mentioned above were used as received. Deionized water (DIW) was used throughout the experiment.

2.2. Synthesis of ZnO/ZnS Heterostructures

ZnO/ZnS heterostructures were fabricated as in our previous report.[24] ZnO nanorods were grown on indium tin oxides (ITO) substrates (STN-SI-10, Rs $\leq$ 10 Ω/□, Tr $\geq$ 83%) by a two-step Chemical Bath Deposition (CBD) method. Before growth, the substrates were ultrasonically cleaned for 15 min in acetone, ethanol and DIW in sequence. ITO substrates were pretreated by coating the substrates with a 5 mM solution of $Zn(C_2H_3O_2)_2 \cdot 2H_2O$ dissolved in pure ethanol. In the CBD growth, the aqueous solutions of 0.1 M $Zn(NO_3)_2 \cdot 6H_2O$ and 0.1 M $C_6H_{12}N_4$ were first prepared and mixed together. The pretreated ITO substrates were immersed into the aqueous solution at 93 °C for 6 h to get ZnO nanorods. ZnS layer was deposited on ZnO nanorods by SILAR method. ZnO nanorods were immersed in a 0.1 M $Zn(NO_3)_2$ solution for five minutes. They were then rinsed with distilled water and immersed in a 0.1 M Na_2S solution for another five minutes followed by another rinsing with distilled water. Samples ZnO/ZnS(5) and ZnO/ZnS(10) and ZnO/ZnS(15) were synthesized via this method and the process were repeated for 5, 10 and 15 times respectively.

2.3. Photocatalytic Activity Mensurements

Rhodamine B (RhB) was used to test the photocatalytic performance of the as-prepared products. 200 ml RhB aqueous (7 mg/L) was prepared, before turning on the lamp, the RhB solution was magnetically stirred in a dark condition for 60 min. 0.9 cm × 0.9 cm ITO substrates with ZnO/ZnS was added into a cuvette equipped with 7 mg/L RhB solution and then exposed to UV light (250 W high-pressure Hg lamp) for different durations. After a period of time, the RhB solution was analyzed on a Varian UV-vis spectrophotometer (UV-5800PC, Shanghai Metash Instruments Co., Ltd) and the absorption value was recorded. The percentage of degradation is reported as C/C_0. C is main peak of the absorption spectrum of pollutants at each irradiated time interval. C_0 is the absorption of the initial solution when adsorption–desorption equilibrium was achieved.

2.4. Instrumentation

X-ray diffraction (XRD) patterns were recorded by a MAC Science MXP-18 X-ray diffractometer using a Cu target radiation source. EDAX (energy dispersive X-ray analysis) was recorded on a Genesis 2000 EDAX. Scanning electron microscopy (SEM) pictures were collected on XL-30 ESEM FEG SEM. Transmission electron micrographs (TEM) and high-resolution transmission electron microscopy (HRTEM) images were taken on TECNAI F20 transmission electron microscope with a acceleration voltage of 200 kV. The room temperature photoluminescence (PL) measurements were carried out on the Renishaw inVia micro-PL spectrometer. A continuous 325 nm light of a He–Cd laser was used as the excitation source.

3. RESULTS AND DISCUSSION

Figure 1(a) shows the XRD patterns of the ZnO, ZnO/ZnS(5), ZnO/ZnS(10), ZnO/ZnS(15) heterostructures. It can be seen from the curves that the diffraction peaks at 30.5° are from ITO substrate; other peaks match well with the crystal structure of the zinc oxide (ZnO) phase, according to Joint Committee on Powder Diffraction Standards (JCPDS). Particularly, the intensity of the (002) diffraction peak located at 34.65° is the stronger than any other diffraction peaks, which illustrates the highly preferential orientation of ZnO nanorod arrays along *c*-axis.[25] However, no additional peaks related to ZnS were observed in XRD patterns, which is consistent with the report of Wang et al.[26] Because the thickness of ZnS layer are negligible compared with ZnO NRs thickness and the amorphous nature of ZnS, no ZnS peaks can be observed. In order to prove the existence of ZnS layer on ZnO nanorods, EDAS measurement has been taken on ZnO/ZnS(10). As shown in Figure 1(b), it exhibits the presence of the 34.06 at%

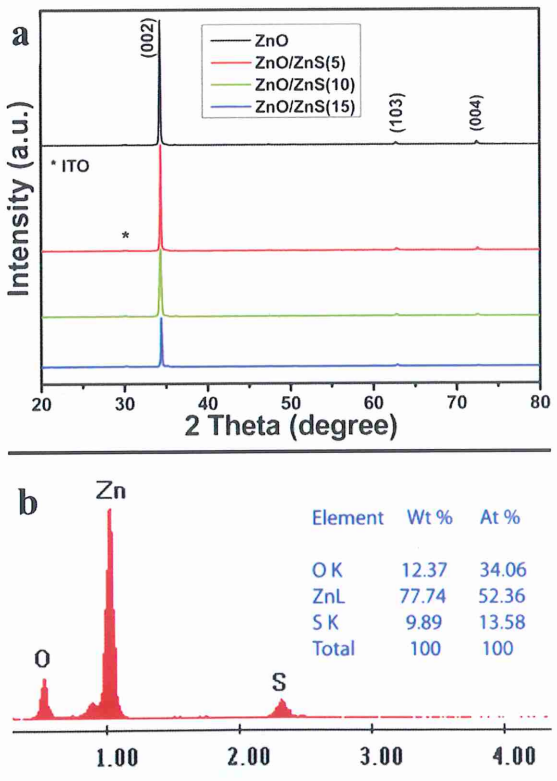

Fig. 1. (a) XRD patterns of ZnO, ZnO/ZnS(5), ZnO/ZnS(10) and ZnO/ZnS(15) heterostructures; (b) EDAS measurement of ZnO/ZnS(10) structure.

O, 52.36 at% Zn and 13.58 at% S elements. The above experiment results prove the formation of ZnO/ZnS heterostructures.

Figure 2(a) is a vertical SEM image of ZnO nanorods grown on ITO substrate. ZnO nanorods are aligned on ITO with a diameter of 100–120 nm, separated by a gap of 10–200 nm. Figures 2(b)–(d) show SEM images of ZnO/ZnS(5), ZnO/ZnS(10) and ZnO/ZnS(15). It can be seen from the figures, the diameter of the structures did not change obviously. However, the surfaces of ZnO nanorods are no longer smooth as in Figure 2(a). ZnO nanorods are wrapped with a thin layer of ZnS nanoparticles, indicating the formation of ZnO/ZnS heterostructures. Figures 2(b)–(d) compares arrays made from different ZnS deposition period. The increase of deposition period makes the ZnO/ZnS heterostructures rougher. A set of High-magnification SEM images are taken to further prove the changes of the sample. As can be seen in Figure 3, the surface of ZnO/ZnS(15) is the roughest.

In order to further discuss the effects of deposition period of the ZnS layer, TEM and high resolution (HRTEM) images of ZnO, ZnO/ZnS(5), ZnO/ZnS(10) and ZnO/ZnS(15) structures were taken as shown in Figure 4. Figure 4(a) shows the TEM image of the ZnO nanorod. The surface of the nanorod is very smooth, which is completely consistent with the SEM image. After repeating the SILAR process for 5 times, a thin layer of ZnS appeared as shown in Figure 4(b). The thickness of ZnS layer was about 13.7 nm. From Figures 4(c) and (d), it can be noticed that with the increased number of SILAR times, the thickness of the ZnS layer was also increased. The thickness of the ZnS layers can be estimated to be 24, 36 nm for ZnO/ZnS(10) and ZnO/ZnS(15) structures respectively. As SILAR times increased, the surfaces of ZnO/ZnS heterostructures became rougher, this is also in agreement with SEM images.

Figures 5(a) and (b) show the HRTEM images of ZnO/ZnS(5) and ZnO/ZnS(10) structure. Both of the figures reveal a lattice fringe of 0.26 nm and 0.31 nm, corresponding to the wurtzite ZnO nanostructure and ZnS nanoparticle. Above experiment data indicating a thin layer of ZnS NPs has uniformly attached on the surface of the ZnO NRs. ZnS NPs have been marked by red circles with average diameter of 4∼5 nm. We can conclude that ZnS NPs have been successfully deposited on the whole surface of the ZnO NRs. Hence, entire length of ZnO NRs forms a ZnO/ZnS cores–shell structure in our experiment process.

The photocatalytic degradation curves of representative samples are clearly shown in Figure 6(a). When UV illumination is introduced, solution color becomes shallow, implicating the decomposition of the RhB. During the previous 30 min under UV light irradiation, degradations take place over the 3 structures. Over 75 min, degradation is still in progress. Among them, the degradation rate of ZnO/ZnS(10) is the fastest. The sufficient contact and interaction between the two ingredients should be primarily responsible for the excellent photocatalytic activity and stability. Firstly, there is a build-in electric field in the composite due to the interaction and the formation of heterostructure between ZnO and ZnS. Besides, the conduction band of ZnS lies at a more negative potential

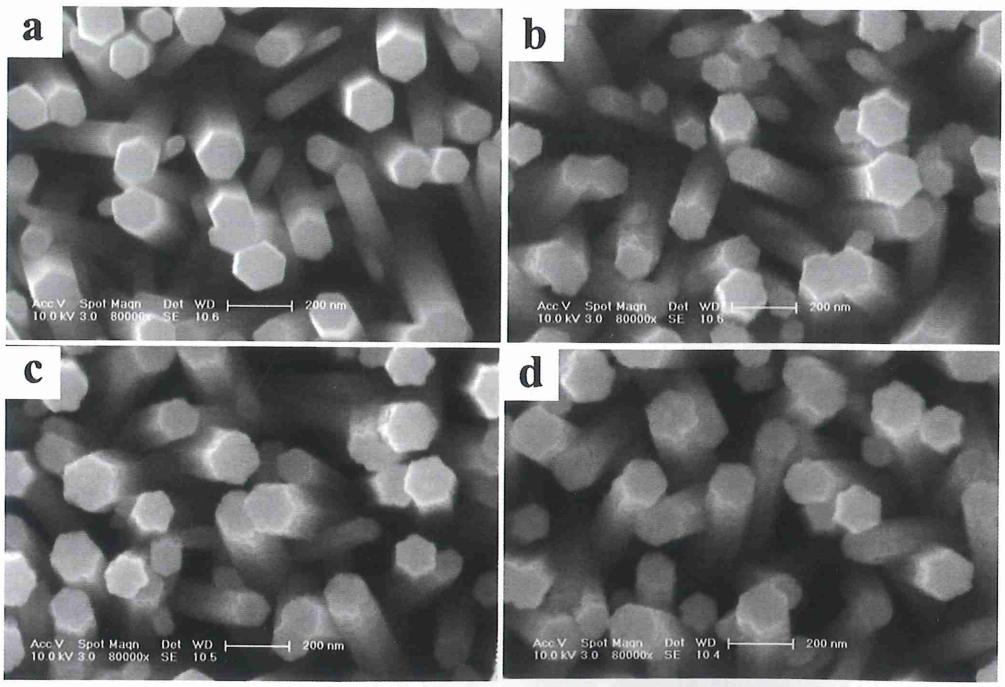

Fig. 2. Vertical-view SEM images of (a) ZnO, (b) ZnO/ZnS(5), (c) ZnO/ZnS(10) and (d) ZnO/ZnS(15) heterostructures.

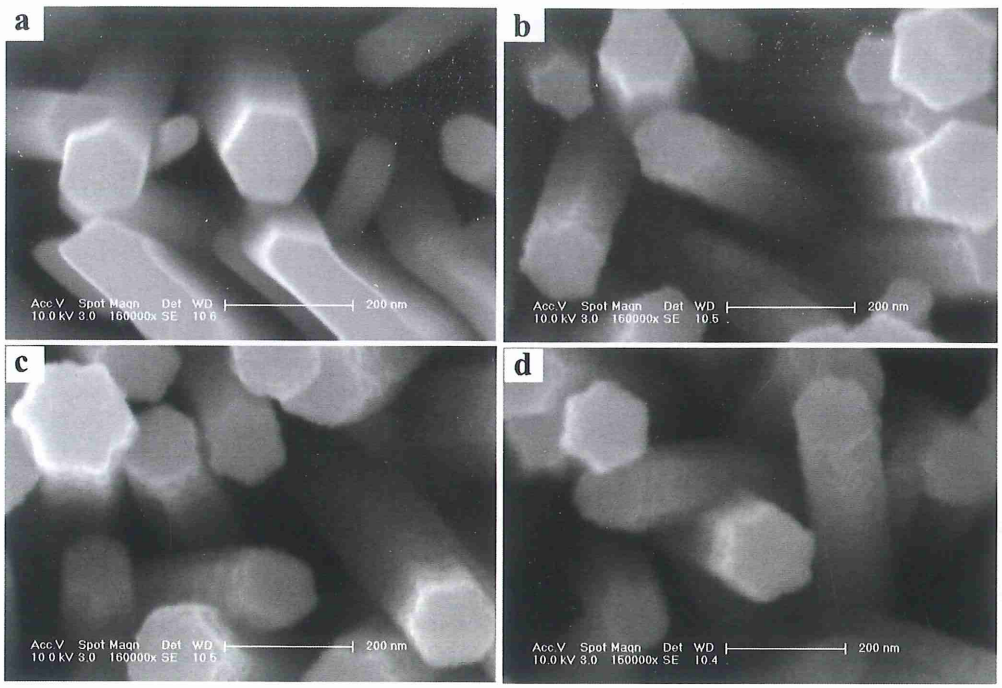

Fig. 3. High-magnification SEM images of (a) ZnO, (b) ZnO/ZnS(5), (c) ZnO/ZnS(10) and (d) ZnO/ZnS(15) heterostructures.

(vs. NHE) than that of ZnO, while the valence band of ZnO is more positive than that of ZnS.15 Hence, after the photogenerated electrons in the valence bands of ZnO core and ZnS shell are excited under UV light irradiation, they deviate from photogenerated holes to the conduction bands and then pass from the conduction band of ZnS shell to that of ZnO core. Meanwhile, the transfer of photogenerated holes occurs from the valence band of ZnO core to that of ZnS shell, which effectively prevents the holes attacking the surface oxygen of ZnO and inhibits the photocorrosion effect. Through this process, the yield and lifetime of charge carriers in the ZnO/ZnS system increase, leading to the more excellent photocatalytic activity of ZnO/ZnS HCSSs than that of pure ZnO and ZnS.[27] For ZnO/ZnS(5) heterostructrue, the poor activity indicates that the activity of the catalysts could not be effectively improved by depositing a thin layer of ZnS. This result can be attributed to the insufficient contact between ZnO and ZnS, which restricts the charge transfer between them. For ZnO/ZnS(15) heterostructrue, the poor activity of the catalysts can be ascribed to the poor electrical conductivity of ZnS compared with ZnO, since it is very hard for photoinduced electrons to pass through ZnS layer when ZnS layer reaches a certain thickness.[24]

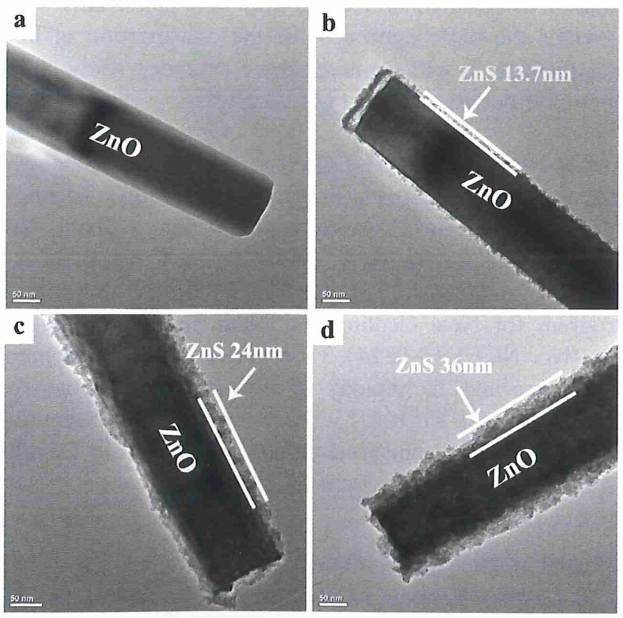

Fig. 4. TEM image of (a) ZnO, (b) ZnO/ZnS(5), (c) ZnO/ZnS(10) and (d) ZnO/ZnS(15) heterostructures.

The normalized room-temperature PL spectra of three samples (ZnO/ZnS(5), ZnO/ZnS(10) and ZnO/ZnS(15)) are shown in Figure 6(b), which was used to investigate the defect of materials and separation efficiency of photogenerated electronehole pairs.[28] As shown in Figure 6(b), all the samples exhibited efficient UV emission and broad visible light emission. The UV emission (~378 nm) is the near band edge emission of ZnO.[29] The visible light emission centered at 540 nm is ascribed to ionized oxygen vacancies, which usually results from the recombination of a photogenerated hole with the singly ionized charge state of these defects.[30] Different visible light emission intensity was displayed in the figure. ZnO/ZnS(10) presents the weakest visible light emission, which indicates that ZnO/ZnS(10) heterostructure

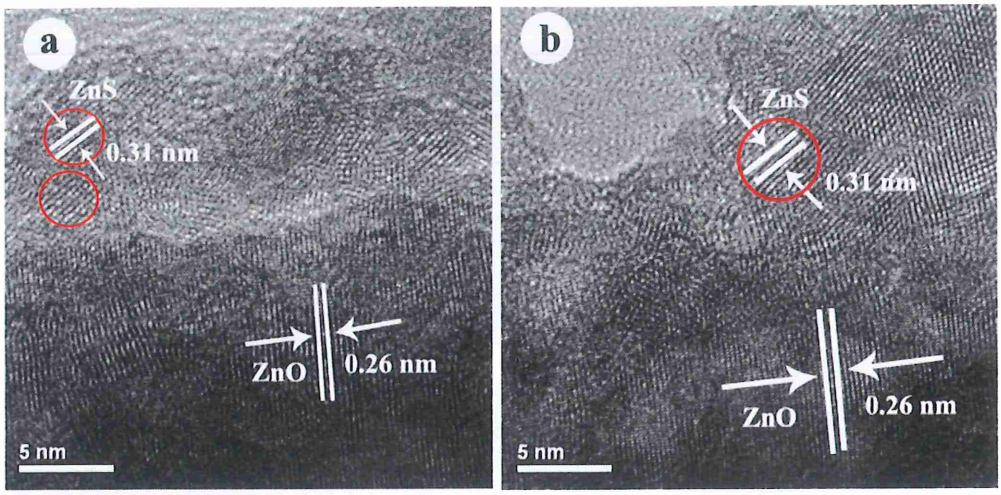

Fig. 5. High resolution (HRTEM) images of ZnO/ZnS(5) and ZnO/ZnS(10).

has better crystalline quality. In addition, weaker visible light emission implies lower recombination of photogenerated electron–hole pairs. In the photocatalysis process, the primary oxidative species are the photogenerated holes, which are able to oxidize H_2O to hydroxyl radicals (•OH) or lead to complete mineralization of organic pollutants. So decreasing serious bulk recombination of photogenerated electron–hole pairs in semiconductors will definitely contribute to the higher photocatalytic activity.[28] That is the main reason why ZnO/ZnS(10) heterostructure have the highest photocatalytic activity.

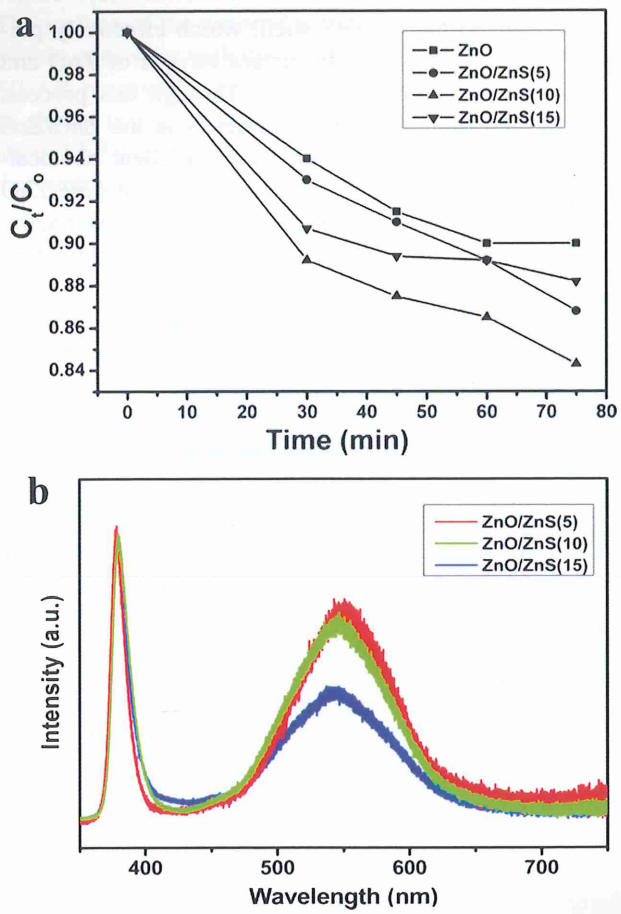

Fig. 6. Photocatalytic activities (a) and normalized room-temperature PL spectra (b) of ZnO, ZnO/ZnS(5), ZnO/ZnS(10) and ZnO/ZnS(15) heterostructures.

4. CONCLUSIONS

In summary, ZnO/ZnS(5), ZnO/ZnS(10) and ZnO/ZnS(10) heterostructures are synthesized by a SILAR method. XRD and EDAS analysis indicates that ZnO/ZnS heterostructures are formed by using ZnO nanorods as template. The ZnO/ZnS(10) structure shows the highest photocatalytic activity due to the better crystalline quality and less recombination of photogenerated electron–hole pairs. This work provides the basic approach for the construction of heterostructures, it will stimulate more extended study about ZnO-base heterostructure photocatalysts.

Acknowledgment: The authors acknowledge financial support from National Programs for High Technology Research and Development of China (Item No. 2013AA032202), National Natural Science Foundation of China (Grant Nos. 11204104, 61178074, and 61475063), Program for New Century Excellent Talents in University (No. NCET-13-0824), Program for the Development of Science and Technology of Jilin province (Item Nos. 201205078 and 20110415), the Twentieth Five-Year Program for Science and Technology of Education Department of Jilin Province (Item No. 20140147).

References and Notes

1. H. C. Ma, X. H. Cheng, C. Ma, X. L. Dong, X. X. Zhang, M. Xue, X. F. Zhang, and Y. H. Fu, *Int. J. Photoenergy* 2013, 625024 **(2013)**.
2. N. Sobana and M. Swaminathan, *Sep. Purif. Technol.* 56, 101 **(2007)**.
3. M. Mrowetz and E. Selli, *J. Photochem. Photobiol. A* 180, 15 **(2006)**.

4. D. D. Lin, H. Wu, R. Zhang, W. Zhang, and W. Panw, *J. Am. Ceram. Soc.* 93, 3384 (**2010**).
5. C. T. Sun and D. F. Xue, *Sci. Adv. Mater.* 5, 909 (**2013**).
6. C. B. Zhang, K. Y. Li, S. Y. Song, and D. F. Xue, *Chem. Eur. J.* 19, 6329 (**2013**).
7. J. S. Wu and D. F. Xue, *Adv. Mater.* 3, 127 (**2011**).
8. C. B. Zhang, S. H. Zhou, K. Y. Li, S. Y. Song, and D. F. Xue, *Mater. Focus* 2, 11 (**2013**).
9. K. Y. Li, P. C. Yan, and D. F. Xue, *Mater. Focus* 2, 143 (**2013**).
10. C. T. Sun and D. F. Xue, *J. Phys. Chem. C* 117, 5505 (**2013**).
11. F. Xu, Z. Y. Yuan, G. H. Du, T. Z. Ren, C. Bouvy, M. Halasa, and B. L. Su, *Nanotechnology* 17, 588 (**2006**).
12. Y. Tak, H. Kim, D. Lee, and K. Yong, *Chem. Commun.* 38, 4585 (**2008**).
13. X. Cao, P. Chen, and Y. Guo, *J. Phys. Chem. C* 112, 20560 (**2008**).
14. K. S. Leschkies, R. Divakar, J. Basu, E. Enache-Pommer, J. E. Boercker, C. B. Carter, U. R. Kortshagen, D. J. Norris, and E. S. Aydil, *Nano Lett.* 7, 1793 (**2007**).
15. J. Y. Kim and F. E. Osterloh, *J. Am. Chem. Soc.* 127, 10152 (**2005**).
16. Z. Liu, J. Deng, J. Deng, and F. Li, *Mater. Sci. Eng. B* 150, 99 (**2008**).
17. S. Sakthivel, S. U. Geissen, D. W. Bahnemann, V. Murugesan, and A. Vogelpohl, *J. Photochem. Photobiol. A* 148, 283 (**2002**).
18. K. Asokan, J. Y. Park, S. W. Choi, S. S. Kim, *Nanoscale Res. Lett.* 5, 747 (**2010**).
19. H. Y. Yang, S. F. Yu, S. P. Lau, X. Zhang, D. D. Sun, and G. Jun, *Small* 5, 2260 (**2009**).
20. C. L. Yan and D. F. Xue, *J. Phys. Chem. B* 110, 25850 (**2006**).
21. J. S. Hu, L. L. Ren, Y. G. Guo, H. P. Liang, A. M. Cao, L. J. Wan, and C. L. Bai, *Angew. Chem. Int. Ed.* 44, 1269 (**2005**).
22. Y. J. Hsu, S. Y. Lu, and Y. F. Lin, *Adv. Funct. Mater.* 15, 1350 (**2005**).
23. D. P. Wu, Y. Jiang, Y. F. Yuan, J. S. Wu, and K. Jiang, *J. Nanopart. Res.* 13, 2875 (**2011**).
24. Y. F. Sun, J. H. Yang, L. L. Yang, J. Cao, M. Gao, Z. Q. Zhang, and Z. Wang, H. Song, *J. Solid State Chem.* 200, 258 (**2013**).
25. Z. Gu, M. P. Paranthaman, J. Xu, and Z. W. Pan, *ACS Nano* 3, 273 (**2009**).
26. K. Wang, J. J. Chen, Z. M. Zeng, J. Tarr, W. L. Zhou, Y. Zhang, Y. F. Yan, S. C. Jiang, J. Pern, and A. Mascarenhas, *Appl. Phys. Lett.* 96, 123105 (**2010**).
27. W. Chen, H. Ruan, Y. Hu, D. Z. Li, Z. X. Chen, J. J. Xian, J. Chen, X. Z. Fu, Y. Shao, and Y. Zheng, *Cryst. Eng. Comm.* 14, 6295 (**2012**).
28. X. Y. Li, J. Wang, J. H. Yang, J. H. Lang, J. Cao, F. Z. Liu, H. G. Fan, M. Gao, and Y. H. Jiang, *Mater. Chem. Phys.* 141, 929 (**2013**).
29. T. Onuma, N. Sakai, T. Igaki, T. Yamaguchi, A. A. Yamaguchi, and T. Honda, *J. Appl. Phys.* 112, 063509 (**2012**).
30. P. Yang, H. Q. Yan, S. Mao, R. Russo, J. Johnson, R. Saykally, N. Morris, J. Pham, R. He, and H. J. Choi, *Adv. Funct. Mater.* 12, 323 (**2002**).

Received: 10 November 2014. Revised/Accepted: 17 November 2014.